Synergistic effect of surface phase junction and surface defects on enhancing the photocatalytic performance of $BiPO_4$

Xianyong Feng, Peifang Wang, Jin Qian, Yanhui Ao ✉, Chao Wang, Jun Hou

Key Laboratory of Integrated Regulation and Resource Development on Shallow Lakes, Ministry of Education, College of Environment, Hohai University, Nanjing 210098, People's Republic of China
✉ *E-mail: andyao@hhu.edu.cn*

Published in Micro & Nano Letters; Received on 22nd August 2017; Revised on 17th December 2017; Accepted on 2nd February 2018

In this work, defective $BiPO_4$ with surface phase junction (BPJ) was synthesised using a facile ball-milling method. The phase composition of BPJ was found to include monazite monoclinic $BiPO_4$ and monoclinic $BiPO_4$. Surface defects on BPJ could be controlled by changing ball-milling conditions. The optimal sample exhibited significantly enhanced photocatalytic performance compared with $BiPO_4$ and BPJ under ultraviolet light irradiation. The enhancement of photocatalytic performance was due to the synergistic effect of the surface phase junction and surface defects, which significantly improved the separation and transfer efficiency of photogenerated charges.

1. Introduction: $BiPO_4$ is the widely studied photocatalyst, owing to its low cost, low toxicity, stability and good photoelectric performance. $BiPO_4$ nanocrystals have shown better photocatalytic activity for the degradation of methylene blue (MB) than P25 titania [1]. However, the wide bandgap of $BiPO_4$ (~4.6 eV) narrows the light response range ($\lambda < 300$ nm) and limits the transmission efficiency of photoinduced charge carriers [2]. It is therefore necessary to find an effective method of improving the photocatalytic performance and expanding the photoresponse range. $BiPO_4$ has three main crystal phases including hexagonal $BiPO_4$ (hBP), monazite monoclinic $BiPO_4$ (nBP) and monoclinic $BiPO_4$ (mBP), of which nBP shows the best photocatalytic activity [3]. It has been reported that the surface phase junction between different phases can enhance the separation and transfer efficiency of photogenerated charges [4]. However, the lower energy utilisation and photoinduced charge transfer efficiency of pure phase $BiPO_4$ limit the potential of surface phase junction.

Previous studies have shown that surface defects have unique advantages in terms of improving optical performance and charge transfer efficiency [2, 5, 6]. In general, defects can be divided into two categories, including surface defects and bulk defects [7]. Both types of the defect can capture photogenerated charges, however surface defects can quickly release photogenerated charge. This temporary capture process can promote the separation of photogenerated electrons and holes [8]. Moreover, the surface defects can serve as adsorption sites for H_2O and O_2 and these adsorbates can instantaneously react with photogenerated charges to produce ·OH and $\cdot O_2^-$, thus enhancing photocatalytic activity [2]. Surface defects have been studied in many photocatalysts such as TiO_2 [9, 10], $BiPO_4$ [11, 12], ZnO [13, 14] and Bi_2WO_6 [15] synthesised via vacuum deoxidation, controllable hydrogen reduction and high-temperature calcination under reducing atmosphere. Although these synthetic approaches have certain advantages, their harsh and dangerous reaction conditions hinder their potential application. In contrast, ball milling has been shown to be a facile way to introduce surface defects [9, 11, 13]. The lack of reports on the synergistic effect of the surface phase junction and surface defects of $BiPO_4$ has motivated this study.

In this work, $BiPO_4$ with surface phase junction (BPJ) with mixed phases of nBP and mBP was prepared using a facile high-temperature calcination method. Defective BPJ (DBPJ) was then achieved via ball milling with controlled milling rate and time. The effects of the surface phase junction and surface defects on the crystallisation, morphology, and optical, photoelectric and photocatalytic performance of the obtained samples were investigated. The mechanism for the synergistic effect of the surface phase junction and surface defects on enhancing photocatalytic performance was also discussed in depth.

2. Fabrication: In a typical $BiPO_4$ and BPJ preparation procedure, 4.85 g (10 mmol) of Bi $(NO_3)_3{\cdot}5H_2O$ was added to 900 ml of 10% aqueous glycerol solution. The mixture was sonicated to ensure complete dissolution of Bi $(NO_3)_3{\cdot}5H_2O$ and the resulting white suspension was stirred for 1 h. The white precipitate was then separated from the suspension by centrifugation, and washed several times using deionised water and ethanol. The precipitate was dried at 120°C for 12 h to give $BiPO_4$ as a white powder. BPJ was prepared by calcining $BiPO_4$ in air at 500°C for 6 h in a muffle furnace.

To prepare DBPJ, 1.0 g of BPJ and 2.0 ml of ethanol were added to an agate jar equipped with different sizes of agate balls. The mixture was then ball milled at 300 rpm for different time periods on a QM-QX12 omnidirectional planetary ball mill. The agate jar was dried under atmospheric conditions to remove ethanol and the obtained samples were identified as DBPJ. Different reference samples ball milled for 1 h at different specific rates were also prepared using the same method.

3. Results and discussion: The crystallisation and phase composition of the samples were investigated by X-ray diffraction (XRD). As shown in Fig. 1, all of the characteristic diffraction peaks of pure $BiPO_4$ were consistent with hBP (JCPDS Card No. 015-0766) and no impurity peaks were observed [16]. After BPJ was synthesised by calcining $BiPO_4$ at 500°C, the main crystalline phases were converted to nBP (JCPDS Card No. 089-0287) [5]. At the same time, a few faint diffraction peaks attributed to mBP (JCPDS Card No. 077-2208) appeared, indicating that a mixture of nBP and mBP was formed [4, 17]. It is clear that the main phase structure of BPJ was unchanged by increased ball-milling rate. However, it is evident that the characteristic diffraction peaks of mBP decreased with increasing milling rate. When the ball-milling rate reached 400 rpm, the characteristic diffraction peaks of mBP were no longer detected. This observation could be due to high-speed ball milling destroying the surface structure of BPJ, which includes the structure of the surface phase junction. This could be a key factor in photocatalytic activity.

doi: 10.1049/mnl.2017.0620

Transmission electron microscopy (TEM) and high-resolution TEM (HRTEM) were used to characterise the morphology and microstructure of the obtained samples. As shown in Fig. 2*a*, pure $BiPO_4$ presented uniform and cuboid shaped particles, and the lattice fringes could be clearly observed. The spacing between adjacent lattice fringes was 0.221 nm which is consistent with the (202) d-spacing of hBP (JCPDS Card No. 015-0766). From Fig. 2*b*, it can be seen that the morphology of BPJ was unchanged compared with $BiPO_4$ and the lattice fringes were still clearly visible after calcination at 500°C. However, it is clear that two different lattice fringes appeared on the crystal. The two different lattice spacings were 0.213 and 0.285 nm, which were indexed to the (−313) d-spacing of nBP (JCPDS Card No. 089-0287) and the (120) d-spacing of mBP (JCPDS Card No. 077-2208), respectively. It was therefore concluded that the surface phase junction between nBP and mBP was generated. As shown in Fig. 2*c*, the TEM images of DBPJ indicated that the uniform cuboid shapes were destroyed by ball-milling, and smaller irregular shaped particles were formed. In addition, two different lattice fringe spacings (0.260 and 0.320 nm) were observed, which are attributed to the (−202) d-spacing of nBP (JCPDS Card No. 089-0287) and the (101) d-spacing of mBP (JCPDS Card No. 077-2208). In addition, lattice defects and plane defects were simultaneously observed in the (−202) plane of nBP and the (101) plane of mBP. These observations were attributed primarily to the formation of defects in the course of ball milling [13].

Ultraviolet–visible (UV–Vis) diffuse reflectance absorption (DRS) was used to investigate the optical properties of $BiPO_4$, BPJ and DBPJ, and the obtained spectra are shown in Fig. 3*a*. It is clear that only pure $BiPO_4$ responds to UV light and its absorption edge is located at ~300 nm. After formation of the surface phase junction, the absorption edge of BPJ was red shift by ~50 nm, which extended it to ~350 nm. Moreover, the absorption intensity of BPJ between 275 and 350 nm was also significantly strengthened. Compared with unprocessed BPJ, ball milling caused a further red shift of the absorption edge and enhancement of absorption intensity, in both the UV and visible wavelength ranges. This indicates that the synergistic effect of the surface phase junction and surface defects can effectively expand the absorption edge and enhance the absorption performance of $BiPO_4$. The inset images of Fig. 3*a* show that the colour of the samples changed from pure white $BiPO_4$ and BPJ to light brown for DPBJ, which is related to the formation of defects [2, 12]. The bandgaps of the obtained samples were estimated from UV-Vis DRS plots using the following equation [18]:

$$A(hv - Eg)^{n/2} = ahv. \quad (1)$$

where A, a, h, v and Eg represent a constant, the absorption coefficient, the Planck constant, the light frequency and the bandgap energy, respectively. Generally, n depends on the type of optical transition of semiconductor. For $BiPO_4$, the n value is 4 because it shows the characteristics of indirect transitions [16]. The plots of $(ahv)^2$ versus (hv) are shown in Fig. 3*b*, the bandgap energies of $BiPO_4$ and PBJ were estimated to be 4.5 and 4.32 eV, respectively. It was therefore concluded that the surface phase junction could induce a lower $BiPO_4$ bandgap energy and result in better photocatalytic activity.

XPS was used to investigate the surface elemental composition of DBPJ and the spectra are shown in Fig. 4. The survey scan (Fig. 4*a*) clearly demonstrates that DBPJ is mainly composed of C, O, P and Bi. Fig. 4*b* shows that the P 2p XPS spectrum presented a wide peak at 131.8 eV, indicating the presence of P in P^{5+} oxidation state in PO_4^{3-} [19, 20]. The O 1s spectrum (Fig. 4*c*) showed a single broad peak at 530.6 eV, which is related to the lattice oxygen in PO_4^{3-} [18]. The high-resolution XPS spectrum of Bi4f (Fig. 4*d*) showed two pairs of peaks, which were attributed to Bi $4f_{5/2}$ and Bi $4f_{7/2}$, respectively. The binding energies at 165.2 and 159.6 eV suggested the existence of Bi^{3+} [20]. The lower binding energies at 164.0 and 158.7 eV are attributed to low charge Bi ions which may be associated with the generation of oxygen defects [21]. The charge reduction caused by the generation of oxygen defects also occurs in BiOCl, which is related to the presence of Bi^{3-x}

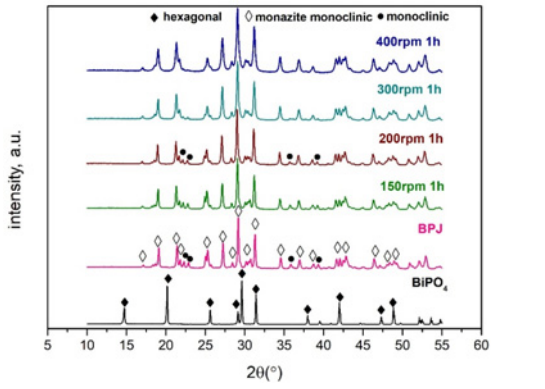

Fig. 1 *XRD patterns of $BiPO_4$, BPJ and BPJ ball-milled at different rates for 1 h*

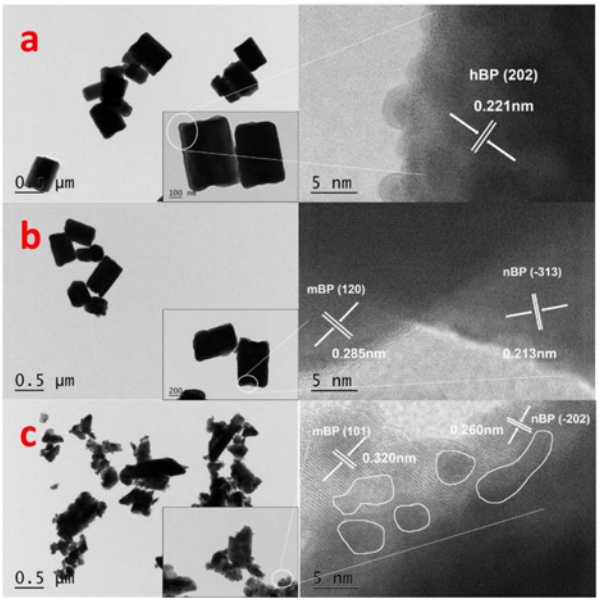

Fig. 2 *TEM and HRTEM images*
a $BiPO_4$
b BPJ
c DBPJ

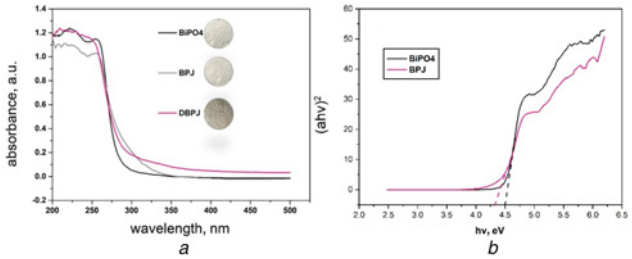

Fig. 3 *Optical properties of different samples*
a UV–Vis DRS spectra of $BiPO_4$, BPJ and DBPJ; Inset images are the corresponding photograph
b The plots of $(ahv)^2$ versus (hv) for $BiPO_4$ and BPJ

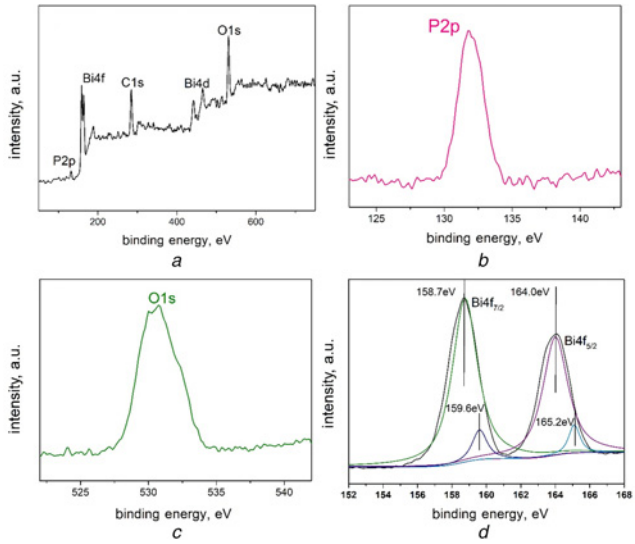

Fig. 4 *XPS spectra of DBPJ*
a Survey scan
b P2p
c O1s
d Bi4f

[22–24]. These observations may indicate the presence of oxygen defects in the obtained samples.

In order to more directly prove the existence of defects, electron paramagnetic resonance (EPR) spectroscopy was carried out at 110 K. As can be seen in Fig. 5, a distinct and prominent peak at *g* value 2.00103 was observed in the DBPJ spectra, which had significantly greater intensity than those in the spectra of $BiPO_4$ and BPJ. It has been reported that *g* values in the range 2.001–2.004 are indicative of surface oxygen defects [2, 11, 12]. The EPR results combined with the HRTEM and XPS findings support the conclusion that the ball-milling process caused the formation of defects in BPJ.

The photocatalytic performance of the obtained samples was investigated using MB degradation under UV light irradiation. As shown in Fig. 6*a*, the photocatalytic degradation of MB by pure $BiPO_4$ was 37% in 30 min. For BPJ, MB degradation was 68% because of the formation of the surface phase junction. After ball milling at 300 rpm, the photocatalytic efficiency of samples increased with increasing ball-milling time, but decreased when the time exceeded 1 h. Fig. 6*b* shows that the photocatalytic degradation of MB increased with increasing ball-milling rate until the ball-milling rate reached 200 rpm. The BPJ ball milled at 200 rpm for 1 h clearly exhibited enhanced photocatalytic performance. The reason for improvement in photocatalytic performance is attributed to: (i) the formation of surface phase junction between nBP and mBP, which could promote the separation and

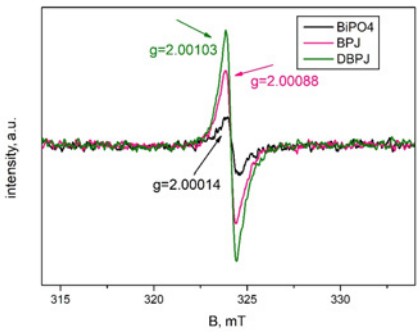

Fig. 5 *EPR spectra of $BiPO_4$, BPJ and DBPJ at 110 K*

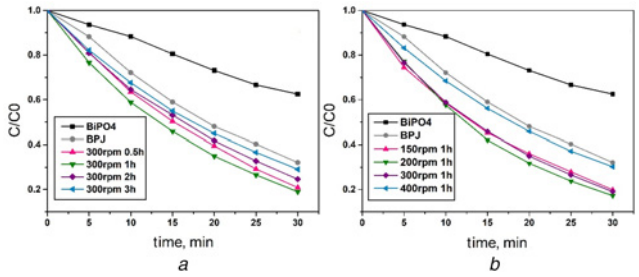

Fig. 6 *Concentration evolution of MB degradation under UV light irradiation*
a By $BiPO_4$, BPJ and samples ball milled at 300 rpm for different time
b By $BiPO_4$, BPJ and samples ball milled at different rate for 1 h

transfer efficiency of photogenerated charge carriers; (ii) the formation of defects on nBP and mBP, which could improve the optical performance of samples and the transfer efficiency of photogenerated charge carriers. It is therefore concluded that the synergistic effect of the surface phase junction and surface defects can enhance photocatalytic performance under UV light irradiation.

A trapping experiment was carried out to identify what kind of active species plays the major role in the photocatalytic degradation of MB. Tertiary butyl alcohol (tert-butanol), p-benzoquinone and ethylenediamine tetraacetic acid disodium salt (EDTA-Na_2) were chosen as the scavengers of hydroxyl radicals (OH), superoxide radicals (O_2^-) and holes (h^+), respectively [13]. As shown in Fig. 7, when these three scavengers were added, the degradation efficiency declined in varying degrees. This indicated that ·OH, $\cdot O_2^-$ and h^+ were involved in the photocatalytic degradation reaction. It was noticed that the most significant decline in degradation occurred when tert-butanol was added. This indicates that ·OH radicals played a major role in the photocatalytic degradation of MB. The addition of EDTA-Na_2 also caused a clear decline in the photocatalytic degradation, which revealed that h^+ also played an important role in the photocatalytic degradation reactions. When p-benzoquinone was added, the degradation rate showed only a small change, which suggests that $\cdot O_2^-$ had a negligible effect on the degradation reaction.

It is well understood that photocatalytic activity is closely related to the transfer efficiency of photogenerated charge carriers, which can be visualised by photocurrent. As shown in Fig. 8, the photocurrent responses were uniform and reversible at lamp-on and lamp-off for all samples. The photocurrent density of pure $BiPO_4$ was the weakest, and by comparison, that of BPJ was enhanced, which revealed that the surface phase junction could enhance the transfer efficiency of photogenerated charge carriers. The photocurrent density was further improved with increasing ball-milling rate. This suggests that the synergistic effect between

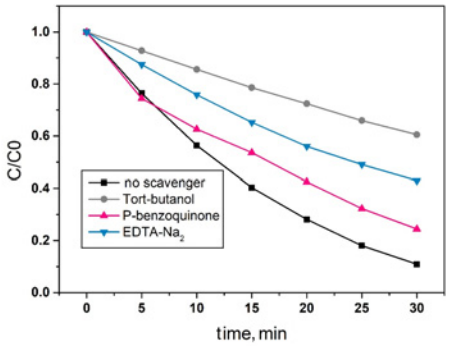

Fig. 7 *Effect of scavengers on the photocatalytic degradation of MB over DBPJ*

doi: 10.1049/mnl.2017.0620

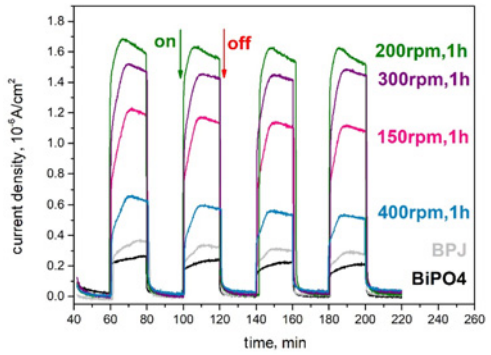

Fig. 8 *Photocurrent of $BiPO_4$, BPJ and BPJ ball milled at different rates for 1 h*

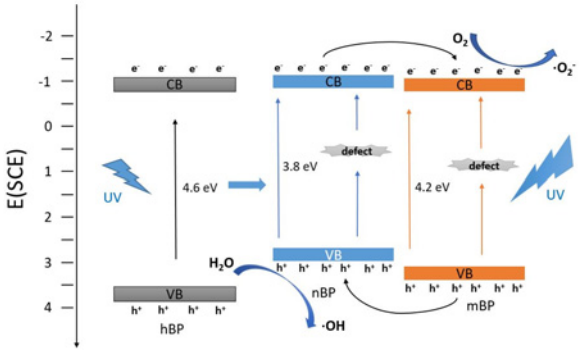

Fig. 10 *Proposed photocatalytic mechanism for DBPJ under UV light irradiation*

the surface phase junction and defects can significantly enhance the transfer efficiency of photogenerated charge carriers. When the ball-milling rate exceeded 200 rpm, the photocurrent density decreased, which was due to the destruction of the surface phase junction structure and the formation of bulk defects caused by high ball-milling rate [11].

Photoluminescence (PL) spectra are an important indication of the separation efficiency of photogenerated charges. High PL intensity indicates a high recombination rate of photogenerated charges [25]. The PL spectra of $BiPO_4$, BPJ and DBPJ are shown in Fig. 9. It was found that the characteristic emission peaks appear at ~414 and 464 nm for all samples. The PL intensity of BPJ was lower than that of $BiPO_4$, suggesting that the surface phase junction improved the separation efficiency of the photogenerated charges. DBPJ exhibited the lowest PL intensity, which indicates that the synergistic effect of the surface phase junction and surface defects could significantly enhance the separation efficiency of photogenerated charges.

Based on the above results and the band position of $BiPO_4$ with mixed phases that has been reported [4], a proposed photocatalytic mechanism for DBPJ under UV light irradiation is shown in Fig. 10. In comparison with DBPJ, the wide bandgap of hBP limited the light absorption and utilisation efficiency. In addition, the low separation and transfer efficiency of the photoinduced charges also hindered the photocatalytic process of hBP. After the formation of surface phase junction between nBP and mBP, the narrower bandgap was introduced at the same time. The conduction band (CB) energy of nBP was the lowest, which caused transfer of photogenerated electrons towards the CB of mBP. The valence band (VB) energy of mBP was higher than that of nBP, therefore the photogenerated holes of mBP transferred to VB of nBP. This transfer process significantly improved the separation efficiency of photogenerated charge. At the same time, the surface defects including oxygen defects on nBP and mBP formed defects states in the bandgap, which further promoted the transfer of electrons towards CB. The electrons and holes reacted with O_2 and H_2O to form $\cdot O_2^-$ and ·OH, respectively. Meanwhile, the surface defects could serve as active sites to improve the photocatalytic reaction. Therefore, the synergistic effect between the surface phase junction and surface defects can significantly improve separation and transfer efficiency of photogenerated charges thus enhancing photocatalytic performance.

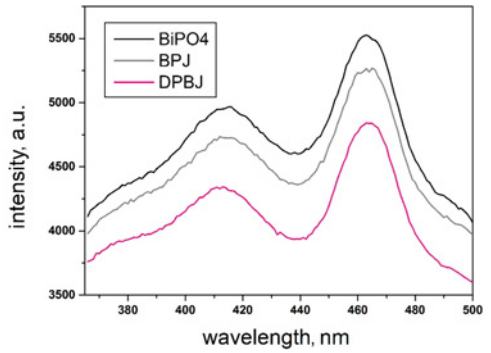

Fig. 9 *PL spectra of $BiPO_4$, BPJ and DBPJ*

4. Conclusion: In summary, DBPJ was synthesised via a facile ball-milling method. The XRD patterns revealed that the surface phase junction between nBP and mBP was formed by high-temperature calcination. The results of HRTEM, XPS and EPR characterisation indicated that surface defects including oxygen defects were formed on both the nBP and mBP. The DBPJ system showed enhanced photocatalytic performance under UV light irradiation. The rate constant k for photocatalytic degradation of MB by the optimal sample, under UV light irradiation, was 3.7 and 1.6 times higher than those of $BiPO_4$ and BPJ, respectively. The enhanced photocatalytic performance was attributed to the synergistic effect of the surface phase junction and surface defects, which could significantly improve separation and transfer efficiency of photogenerated charges.

5. Acknowledgments: The authors are grateful for grants from National Science Funds for Creative Research Groups of China (grant no. 51421006), the Key Program of National Natural Science Foundation of China (grant no. 91647206), the National Science Foundation of China for Excellent Young Scholars (grant no. 51422902), the National Key Plan for Research and Development of China (grant no. 2016YFC0502203), Natural Science Foundation of China (grant no. 51679063) and PAPD.

6 References

[1] Ma W., Zhang L., Qian N., *ET AL.*: 'Size-controlled synthesis of $BiPO_4$ nanostructures and their photocatalytic performances', *Arab. J. Sci. Eng.*, 2014, **39**, (9), pp. 6721–6725

[2] Lv Y., Zhu Y., Zhu Y.: 'Enhanced photocatalytic performance for the $BiPO_{4-X}$ nanorod induced by surface oxygen vacancy', *J. Phys. Chem. C*, 2013, **117**, (36), pp. 18520–18528

[3] Zhao M., Li L., Yang L., *ET AL.*: 'Exploring the unique electrical properties of metastable $BiPO_4$ through switchable phase transitions', *CrystEngComm*, 2013, **15**, (3), pp. 609–615

[4] Zhu Y., Liu Y., Lv Y., *ET AL.*: 'Enhancement of photocatalytic activity for $BiPO_4$ via phase junction', *J. Mater. Chem. A*, 2014, **2**, (32), pp. 13041–13048

[5] Wei Z., Liu Y., Wang J., *ET AL.*: 'Controlled synthesis of highly dispersed $BiPO_4$ photocatalyst with surface oxygen vacancy', *Nanoscale*, 2015, **7**, (33), pp. 13943–13950

[6] Shi B., Yin H., Li T., *ET AL.*: 'Synthesis of surface oxygen-deficient $BiPO_4$ nanocubes with enhanced visible light induced photocatalytic activity', *Mater. Res.*, 2017, **20**, (3), pp. 619–627

[7] Yan J., Wu G., Guan N., *ET AL.*: 'Understanding the effect of surface/bulk defects on the photocatalytic activity of TiO_2: anatase versus rutile', *Phys. Chem. Chem. Phys.*, 2013, **15**, (26), pp. 10977–10978
[8] Kong M., Li Y., Chen X., *ET AL.*: 'Tuning the relative concentration ratio of bulk defects to surface defects in TiO_2 nanocrystals leads to high photocatalytic efficiency', *J. Am. Chem. Soc.*, 2011, **133**, (41), pp. 16414–16417
[9] Zhou X., Liu N., Schmidt J., *ET AL.*: 'Noble-metal-free photocatalytic hydrogen evolution activity: the impact of ball milling anatase nanopowders with TiH_2', *Adv. Mater.*, 2016, **29**, (5), p. 1604747
[10] Pei Z., Weng S., Liu P.: 'Enhanced photocatalytic activity by bulk trapping and spatial separation of charge carriers: a case study of defect and facet mediated TiO_2', *Appl. Catal. B-Environ.*, 2016, **180**, pp. 463–470
[11] Zhu Y., Qiang L., Liu Y., *ET AL.*: 'Photocatalytic performance of $BiPO_4$ nanorods adjusted via defects', *Appl. Catal. B, Environ.*, 2016, **187**, pp. 204–211
[12] Lv Y., Liu Y., Zhu Y., *ET AL.*: 'Surface oxygen vacancy induced photocatalytic performance enhancement of a $BiPO_4$ nanorod', *J. Mater. Chem. A*, 2014, **2**, (4), pp. 1174–1182
[13] Chen D., Wang Z., Ren T., *ET AL.*: 'Influence of defects on the photocatalytic activity of ZnO', *J. Phys. Chem. C*, 2014, **118**, (28), pp. 15300–15307
[14] Lv Y., Pan C., Ma X., *ET AL.*: 'Production of visible activity and UV performance enhancement of ZnO photocatalyst via vacuum deoxidation', *Appl. Catal. B, Environ.*, 2013, **138-139**, (28), pp. 26–32
[15] Hou J., Cao S., Wu Y., *ET AL.*: 'Simultaneously efficient light absorption and charge transport of phosphate and oxygen-vacancy confined in bismuth tungstate atomic layers triggering robust solar CO_2 reduction', *Nano Energy*, 2017, **32**, pp. 359–366
[16] Li G., Ding Y., Zhang Y., *ET AL.*: 'Microwave synthesis of $BiPO_4$ nanostructures and their morphology-dependent photocatalytic performances', *J. Colloid Interface Sci.*, 2011, **363**, (2), pp. 497–503
[17] Pan C., Li D., Ma X., *ET AL.*: 'Effects of distortion of PO_4 tetrahedron on the photocatalytic performances of $BiPO_4$', *Catal. Sci. Technol.*, 2011, **1**, (8), pp. 1399–1405
[18] Lin H., Ye H., Chen S., *ET AL.*: 'One-pot hydrothermal synthesis of $BiPO_4/BiVO_4$ with enhanced visible-light photocatalytic activities for methylene blue degradation', *RSC Adv.*, 2014, **4**, (21), pp. 10968–10974
[19] Pan C., Xu J., Wang Y., *ET AL.*: 'Dramatic activity of $C_3N_4/BiPO_4$ photocatalyst with core/shell structure formed by self-assembly', *Adv. Funct. Mater.*, 2012, **22**, (7), pp. 1518–1524
[20] Xu H., Xu Y., Li H., *ET AL.*: 'Synthesis, characterization and photocatalytic property of $AgBr/BiPO_4$ heterojunction photocatalyst', *Dalton Trans.*, 2012, **41**, (12), pp. 3387–3394
[21] Ye L., Deng K., Xu F., *ET AL.*: 'Increasing visible-light absorption for photocatalysis with black BiOCl', *Phys. Chem. Chem. Phys.*, 2012, **14**, (1), pp. 82–85
[22] Jiang J., Zhang L., Li H., *ET AL.*: 'Self-doping and surface plasmon modification induced visible light photocatalysis of BiOCl', *Nanoscale*, 2013, **5**, (21), pp. 10573–10581
[23] Ye L., Jin X., Leng Y., *ET AL.*: 'Synthesis of black ultrathin BiOCl nanosheets for efficient photocatalytic H_2 production under visible light irradiation', *J. Power Sources*, 2015, **293**, pp. 409–415
[24] Kong L., Jiang Z., Lai H.C., *ET AL.*: 'Does noble metal modification improve the photocatalytic activity of BiOCl?', *Prog. Nat. Sci. Mater.*, 2013, **23**, (3), pp. 286–293
[25] Zhang Y., Zhang N., Tang Z.R., *ET AL.*: 'A unique silk mat-like structured Pd/CeO_2 as an efficient visible light photocatalyst for green organic transformation in water', *ACS Sustain. Chem. Eng.*, 2013, **1**, (10), pp. 1258–1266

doi: 10.1049/mnl.2017.0620